Published in final edited form as:
Magn Reson Med. 2013 October ; 70(4): 954–961. doi:10.1002/mrm.24904.

Simultaneous T_1 and B_1^+ Mapping using Reference Region Variable Flip Angle Imaging

Kyunghyun Sung[1,*], **Manojkumar Saranathan**[2], **Bruce L. Daniel**[2], and **Brian A. Hargreaves**[2]

[1]Department of Radiological Sciences, UCLA, Los Angeles, California, USA

[2]Department of Radiology, Stanford University, Stanford, California, USA

Abstract

Purpose—To present a new method that can simultaneously and efficiently measure T_1 and B_1^+ maps using reference region variable flip angle (RR-VFA) imaging.

Methods—Assuming T_1 relaxation time in a reference region such as fat is well characterized, and the reference region sufficiently covers smoothly varying B_1^+ field inhomogeneity, B_1^+ maps can be measured from VFA images, conventionally used for T_1 measurements. Fat-only images from 2-point Dixon acquisitions were used to compute B_1^+ maps, and the B_1^+ maps were compared with ones using the double angle method (DAM) in 22 breast MRI patients at 3T. Additionally, high spatial resolution VFA images were acquired to show T_1 measurements with and without the RR-VFA B_1^+ correction in six patients.

Results—RR-VFA is able to generate reliable B_1^+ maps, similar those using the conventional DAM. This simultaneous T_1 and B_1^+ mapping can also be used to reduce T_1 estimation errors, where T_1 maps have more uniform fibroglandular tissue T_1 and better depiction of heterogeneous T_1 of breast masses.

Conclusion—A new method that can measure both T_1 and B_1^+ maps based on Dixon VFA images is described, offering improved T_1 quantification with no scan time penalty.

Keywords

B_1 field inhomogeneity; T_1 mapping; Quantitative DCE-MRI; Breast imaging; High-field MRI

INTRODUCTION

Dynamic contrast-enhanced MRI (DCE-MRI) is a commonly used method in the diagnosis of cancer (1,2), which typically acquires a time series of T1-weighted images before and after injection of gadolinium contrast agent (CA). Pre-contrast T_1 measurements are necessary to convert the signal intensities from T1-weighted images into CA concentration (3). CA uptake curves can be used to extract quantitative or semi-quantitative microvascular properties using pharmacokinetic modeling (4,5), which can potentially provide predictive, prognostic and pharmacodynamic response biomarkers for cancers (6–8).

One common method to measure T_1 is variable flip angle (VFA) imaging, also known as Driven Equilibrium Single-Pulse Observation of T1 (DESPOT1), which uses several short TR spoiled gradient-echo (SPGR) acquisitions with varying flip angles (9–11). Using the SPGR signal equation and linear fitting, T_1 maps can be estimated. VFA imaging is widely

*Correspondence to: Kyunghyun Sung, PhD, Department of Radiological Sciences, 300 UCLA Medical Plaza, Suite B119, Los Angeles, CA 90095, Phone: (310) 267-6842, Fax: (310) 825-9118, ksung@mednet.ucla.edu.

used in DCE-MRI since it is highly time-efficient and allows rapid 3D volumetric T_1 mapping with the same pulse sequence used to measure contrast uptake (9,12). Even though many efforts have been made to improve the accuracy of VFA imaging, VFA methods seem to be less accurate in vivo due to their high sensitivity to any flip angle variations (13–15).

Non-uniformity of transmit radiofrequency (B_1^+) field can lead to flip angle variations from the prescribed flip angle. The B_1^+ inhomogeneity tends to become more severe at higher field strengths. At 3 Tesla, noticeable B_1^+ variations over the chest (around 30 – 50%) have been observed by many studies (16–19). Therefore, any B_1^+ variation should be carefully addressed for any quantitative or multi-parametric imaging at 3T or higher field strengths, and the accuracy of VFA can be improved by compensating for the B_1^+ variation (13,15,20).

Separate measurements of T_1 and B_1^+ prolong the clinical protocols. More importantly, many centers have limited ability to include time-efficient methods for B_1^+ mapping, and there also exist previous T_1 data without acquiring B_1^+ mapping. Similar to VFA, the double-angle method (DAM) acquires images with two flip angles but requires long TRs ($TR \gg T_1$) to avoid dependence on T_1 (21), or requires a B_1-insenstive saturation pulse (17,22). In contrast, VFA intentionally includes the dependence of TR on T_1 to compute T_1 values without assuming any B_1^+ variation. If T_1 is known on a well-characterized and well-separated reference region (e.g., lipid tissue), the VFA signal equations can be used to estimate B_1^+ variation in the reference tissue (23), and possibly, the entire B_1^+ variation can be estimated by interpolating using the B_1^+ variation in the reference tissue.

In this work, we describe a novel way to simultaneously measure T_1 and B_1^+ maps using reference region VFA (RR-VFA) imaging. Assuming the T_1 relaxation time for breast fat tissue (reference region) is globally uniform and well characterized at 3T (24), we use a two-point Dixon algorithm (25) to generate fat-only images and assign a known fat T_1 value to a ratio of signal magnitudes for computing B_1^+ variation. Secondly, assuming the B_1^+ field inhomogeneity is smoothly varying across the breast (15,18,19), we apply 3D interpolation to construct the complete B_1^+ variation map. We then compare our B_1^+ maps with those using conventional DAM in 22 breast MRI patients and show differences in T_1 calculation with and without compensating for the B_1^+ variation in six breast MRI patients at 3T.

METHODS

The signal intensity ($I_{\alpha n}$) using SPGR with a nominal flip angle (α_n) can be expressed as:

$$I_{\alpha_n} = M_0 \frac{(\sin\alpha_n(1-E_1))}{(1-E_1\cos\alpha_n)}; \quad [1]$$

where M_0 is the longitudinal magnetization including coil sensitivities and $E_1 = e^{-TR/T1}$. Introducing a relative flip angle variation $B_1(r)$, defined by a ratio between the actual flip angle and the prescribed flip angle (i.e., 1 means the actual flip angle is same as the prescribed flip angle, and 0.5 means 50% reduction in the flip angle), we can express the actual flip angle as $B_1(r)\alpha_n$. A signal ratio of signal magnitudes with two flip angles (α_1 and α_2) for each voxel can be written as:

$$\frac{I_{\alpha 2}(r)}{I_{\alpha 1}(r)} = \frac{\sin(B_1(r)\alpha_2)\cdot(1-E_1\cos(B_1(r)\alpha_1)}{\sin(B_1(r)\alpha_1)\cdot(1-E_1\cos(B_1(r)\alpha_2)}, \quad [2]$$

where r represents spatial position. Provided the fat T_1 is known and is globally uniform, $B_1(r)$ in fatty tissue (r in the reference region) becomes the only unknown in Eq. [2] and can be numerically calculated using the signal ratio for each voxel. Note that any image non-

uniformities (e.g., receive sensitivity) except for the flip angle variation are cancelled out, as they are identical for both magnitude images.

We investigated the accuracy of the RR-VFA B_1^+ measurement with different sets of flip angles and different signal-to-noise ratios (SNRs) using numerical simulations. We simulated fat signal as a function of relative flip angle variation B_1 (from 0.2 to 1.8), based on a published value for fat T_1 of 367 ms (24). To account for any inaccuracies between true and assumed T_1 values in the reference region, we also examined possible B_1^+ measurement errors when there exist variations of the reference region T_1 value. With TR of 4 ms, the Ernst angle for the fat signal was 8.5°. Three sets of signal ratios (5°/10°, 10°/15°, and 5°/15°) were selected to evaluate the signal behavior, and three different noise levels were added to the simulated signal (maximum SNRs were 12, 26 and 74). The accuracy of the esimated B_1 was analyzed using second order statistics: mean and standard deviation (SD).

Figure 1 illustrates the method of generating a final B_1^+ map using RR-VFA. After computing the signal ratio of two fat-only signal magnitudes, we computed a fat-only relative flip angle map using the numerically simulated signal ratio. When the fat-water separation is not perfect, partial-volume effects can cause an error in the flip angle map due to additional T_1 values. This can be reduced by enforcing a smoothing constraint using a quadratic penalty:

$$f(r)=\frac{1}{n_r}\sum_{p\in\delta_r}(B_1(r)-B_1(p))^2, \quad [3]$$

where δ_r is the 3rd-order neighborhood only in the fatty tissue (which, in three dimensions, includes the maximum of 124 voxels (5×5×5 boxcar) surrounding p), and n_r is a total number of voxels in δ_r. We excluded the spatial location r in the flip angle map when the penalty function $f(r)$ becomes more than 0.04.

Secondly, we applied 3D interpolation and reduced the spatial resolution to fill up the non-fat region. The interpolation method fits a surface of the measured fat-only region to the entire three-dimensional data using the *griddata* function in Matlab (R2012b; The Mathworks, Natick, MA). The fitting was based on linear interpolation, but other fitting methods can also be applied. We reduced the spatial resolution by a factor of two in all three directions by applying a Gaussian window in the frequency domain, assuming that B_1^+ field inhomogeneity varies smoothly across the object (15,18,19).

Experiments were performed on 3.0T GE MR 750 systems (GE Healthcare, Waukesha, WI). The axial orientation was chosen for all imaging as it is commonly used in breast MRI, and a large B_1^+ variation is expected from left to right. A body coil was used for B_1 transmission, and the automatic pre-scan values provided by the scanner were used to calibrate B_1 transmission. No transmit RF field shimming is used. This retrospective review and analysis of the VFA data was performed in accordance with a protocol approved by our Institutional Review Board.

The VFA sequence was performed as a part of our standard clinical breast DCE-MRI protocol. We analyzed data on a total of 22 women undergoing clinically indicated breast MRI for a history of known or suspected breast disease, ranging in age between 26 and 73 years (age = 49.9 ± 11.2 years and mass = 60.9 ± 7.4 kg). Based on the official mammographic breast density, rated on a scale of four: fatty (F), scattered fibroglandular densities (S), heterogeneously dense (H), and dense (D), the 22 cases were classified as 6 S, 7 H, and 2 D, with 7 not being assigned. We used a 3D SPGR sequence with a dual-echo bipolar readout, where TEs were chosen to be in- and opposed-phase images (TE = 1.2/2.4

ms), and a two-point Dixon fat-water separation algorithm was used to generate fat- and water-only images (25). We performed the T_1 mapping before DCE-MRI using two flip angles of 6° and 13°, optimized to symmetrically sample the signal curve of fat (T_1 was assumed to be 367 ms (24) and TR = 4.3 ms in simulation). Other imaging parameters were as follows: acquisition matrix size = 256×128×88, slice thickness = 4.2 mm, FOV = 32 cm, and total scan time = 20 sec.

For comparison of B_1^+ measurements, we also measured B_1^+ maps using conventional DAM (21) and used the Bland-Altman plot to show the differences between two B_1^+ mapping methods in 22 subjects. We acquired the B_1^+ maps after post contrast scans to ensure greater T_1 relaxation recovery of all tissue with flip angles of 60° and 120° and TR of 5 sec. Errors due to imperfect 2D slice profiles were corrected in the flip angle calculation (26). We normalized an actual flip angle map by 60° to compute the relative flip angle variation. Other imaging parameters were as follows: echo time (TE) = 2.5 ms, acquisition matrix = 64 × 64, number of slices = 49, slice thickness = 4 mm, field-of-view (FOV) = 44 cm, and total scan time = 9 min.

Lastly, in six additional breast patient cases (age = 52.2 ± 10.4 years and mass = 76.5 ± 13.7 kg), we acquired data with more than two flip angles using high spatial resolution VFA imaging to measure simulataneous T_1 and B_1^+ maps. We used the same dual-echo bipolar readout and selected five flip angles of 2°, 5°, 9°, 13°, and 15°, optimized to symmetrically sample the signal curve of the fibrogladular tissue T_1. We used 5° and 15° fat-only images for B_1^+ maps and used all five flip angles for T_1 maps with compensation for the B_1^+ variation. Other imaging parameters were as follows: acquisition matrix size = 262×308×192, slice thickness = 1.2 mm, TR = 4.3, FOV = 32 cm, and total scan time = 7 min 25 sec.

RESULTS

Numerical Simulation

Figure 2a shows fat signal intensity I_α (mean and SD) as a function of relative flip angle variation with different nominal flip angles (α = 5°, 10° and 15°). We added the same level of Gaussian noise to the simulated signal, accounting for error bars in the plots, and the nominal SNRs (SNRs with no B_1^+ variation) for 5°, 10° and 15° were 21, 26, and 21 respectively. Among all three types of signal ratios, the signal ratio of 5° and 15° (I_5/I_{15}) has the biggest dynamic range with the lowest SD (Fig 2b), possibly resulting in the lowest estimation error. Fig 2c shows the plots between the estimated and true flip angle variation, indicating the estimation error using the signal ratio (Eq. [2]). The solid gray lines are the identity lines. For I_5/I_{15}, the mean of the estimated B_1 becomes very close to the true B_1 with very small SD (SD/mean ranges from 0.6 to 0.8) when the true B_1 is between 0.6 and 1.4, a typical range of B_1^+ variation for breast imaging at 3T (15,18,19).

Figure 3 illustrates the accuracy of the proposed B_1^+ measurement with different SNRs. Three different levels of Gaussian noise have been added to the simulated fat signal, and the nominal SNRs for 15° were 11, 21, and 66. When SNR is extremely low (e.g., less than 15), the measurement becomes slightly biased with the significant noise sensitivity, especially around the high B_1^+ variation range (± 40 %). However, when SNR is marginal (e.g., more than 30), the measurement does not include any systematic bias with the very low measurement SD (i.e., high accuracy and high precision). Note that we can typically expect sufficient SNRs for VFA imaging due to the short T_1 of fat.

Figure 4 shows the effects of assumed reference region T_1 values on the RR-VFA B_1^+ estimation for a true T_1 value of 367 and 1200 ms. When there exists any difference between

the true and assumed T_1 values in the reference region, the numerical signal ratio (Eq. [2]) becomes different from the true signal ratio, and the RR-VFA B_1^+ estimation can be less accurate. Fig 4a shows different signal ratios for ± 5% variations of the true short T_1 (367 ± 18 ms) and long T_1 (1200 ± 60 ms) values. When the assumed reference region T_1 is longer than the true T_1, the proposed method typically underestimates B_1^+ variation, resulting in negative percentage errors, while the shorter T_1 results in positive percentage errors. Fig 4b shows the B_1^+ estimation errors caused by these T_1 variations. Within ± 5% variations of the true T_1, the difference in the signal ratios is subtle, and the B_1^+ estimation error is well within ± 2.5%. Furthermore, with ± 10% and ± 15% variations of the true T_1, the B_1^+ estimation errors are around ± 5% and −7 to +8% for both short and long T_1 values.

Comparison between RR-VFA and DAM

Figure 5 shows examples of B_1^+ maps, shown as relative flip angle distribution (%), in subjects with heterogeneously dense (Fig 5a) and dense (Fig 5b) breasts using DAM and RR-VFA. Among the four levels of breast density rated based on the mammogram reports (fatty, scattered fibroglandular densities, heterogeneously dense, and dense), those two cases were considered to include the least amount of the fatty tissue. The B_1^+ maps using two different methods are qualitatively well matched with each other. There exists a small region in the heart that shows a slight disagreement between two methods (see the arrows) because the heart does not include enough fatty tissue, but the heart was not the tissue of interest in our study. In all 22 cases, the proposed method was able to robustly generate B_1^+ maps, qualitatively well matched with those using DAM. Note that 3D imaging was used for RR-VFA, whereas multi-slice 2D imaging was used for DAM.

Figure 6 shows the mean and SD of relative B_1^+ variation over the region of interest (ROI) for a single subject (Fig 6a and b), and the Bland-Altman plot comparing the B_1^+ maps over the ROI measured by RR-VFA and DAM in 22 subjects (Fig 6c). We manually defined circular ROIs almost covering each of the whole left and right breasts in the central axial slice. Both methods show similar patterns (mean ± SD) of B_1^+ variation within each breast, and the difference in B_1^+ variation is very small (the 95% confidence interval is ranging from −8.9% to 3%).

Simultaneous T_1 and B_1^+ mapping using RR-VFA

Figure 7 shows representative high spatial resolution T_1 and B_1^+ maps including both fat and fibroglandular tissue. The “water+fat” image is shown in Fig 7a. The T_1 map using conventional VFA imaging, generated by the nominal flip angle of 2°, 5°, 9°, 13°, and 15°, has considerable T_1 differences between the left and right breast (shown in Fig 7b), while the high spatial resolution T_1 map using RR-VFA shows more uniform fibroglandular T_1 across the whole breast (shown in Fig 7d) and better depicts heterogeneous T_1 of several breast masses (see the arrows). We used the 5° and 15° fat-only images for B_1^+ mapping and all five flip angles (water+fat images) for T_1 mapping with compensation for the B_1^+ variation.

Figure 8 shows box plots (median, 25th and 75th percentiles, and lower and upper extremes) of fibroglandular T_1 estimation using VFA and RR-VFA in all six patients. The estimated fibroglandular T_1 values using VFA (without B_1^+ correction) are 1607.3 ± 343.8 ms (mean ± SD) on the left ROI and 799.4 ± 191.2 ms on the right ROI, while the estimated glandular T_1 values using RR-VFA (with B_1^+ correction) are 1262.8 ± 37.2 ms on the left ROI and 1304.0 ± 104.5 ms on the right ROI. The T_1 difference between the left and right fibroglandular ROIs is 50% and is reduced to 3% after correcting for the B_1^+ variation.

DISCUSSION

For simultaneous T_1 and B_1^+ mapping, the proposed method (RR-VFA) relies on two major assumptions: the T_1 value of the reference region is known, and the reference region sufficiently covers the smoothly varying B_1^+ inhomogeneity across the object. With those two assumptions, we were able to measure B_1^+ maps in the reference region (i.e., fatty tissue) and to estimate T_1 maps over the non-reference region (i.e., non-fatty tissue). Furthermore, the proposed method naturally allows improved accuracy of the T_1 estimation by accounting for the estimated B_1^+ variation.

The first major assumption for the proposed method is that the T_1 value for the fatty tissue is globally uniform and well-characterized. For breast fat, the previous study has shown T_1 values are very consistent (366.8 ± 7.8 ms) across five healthy women at 3T (24), especially when the fat and water separation was performed using IDEAL (27). For subcutaneous fat, another study has also shown consistent T_1 values (382 ± 13 ms) across six healthy volunteers at 3T (28). In these stuides, the fat T_1 values are fairly consistent and well within a range of ± 5% variation, where we have shown the proposed method is robust to these T_1 variations. However, there may exist some systematic bias in the fat T_1 measurements largely because different studies have used different measurement methods, especially with and without fat-water separation. Therefore, we believe it is important to carefully verify the assumed fat T_1 to avoid any systematic T_1 bias when different T_1 measurement methods are used in RR-VFA.

The second assumption is that the fatty tissue sufficiently covers the smoothly varying B_1^+ inhomogeneity across the object. This is generally true for breast imaging, but populations who have dense breasts may not have enough fatty tissue to represent the smooth B_1^+ variation across the breasts. In this study, we included 8 heterogeneously dense and 2 dense breast cases but did not find any cases with extremely negligible fatty tissue. This may restrict the use of this method for imaging in other parts of the body. However, recent study also showed B_1^+ variation can be described by a small set of basis (Bessel/Fourier) functions (29), suggesting that even a small reference region can still be effective for B_1^+ mapping if the reference region is well distribued across the object of interest.

We used a two-point Dixon method to identify the fatty tissue in the breast for B_1^+ mapping. We expect other Dixon-based methods (e.g., IDEAL) to yield better fat-water separation, which can reduce fat-water partial volume effects (27). If fat-water separation methods are not available, a manual or semi-manual segmentation method may be alternatively used to locate the pure fat-only region. However, if conventional fat saturation were applied for VFA images, the proposed method would not be directly applicable, since it is not possible to locate the fatty tissue.

Conventional DAM is well known to have a limited dynamic range for reliable B_1^+ measurements (17,21,22). In fact, DAM B_1^+ estimation becomes less reliable when the measured relative B_1^+ variation becomes smaller (i.e., the actual flip angle is smaller than the prescribed flip angle) due to increased noise sensitivity (17). Although we corrected the errors due to an imperfect 2D slice profile for DAM, there may exist other errors, which can be more significant in the right breast than the left breast since the actual flip angles in the right breast are typically lower than the actual flip angles in the left breast (15,19). Nevertheless, both DAM and RR-VFA methods have similar B_1^+ estimates over the breast at 3T.

To measure B_1^+ variation, we have exploited the breast fat tissue as a reference region because the T_1 value of fat is well characterized and is known to be consistent across the different subjects. However, it may be possible to use other tissue as the reference region in

this method, if it has well-characterized T_1 values (e.g., saline implants, pelvic muscle etc), but the reliability of B_1^+ mapping may vary.

The VFA imaging is commonly used in routine clinics to calculate T_1, especially as a part of DCE-MRI protocols. One advantage of the proposed technique is to allow generation of B_1^+ maps in addition to T_1 maps without additional scanning and without much change to the existing protocol. This may alleviate concerns of being its clinical protocol to be time-efficient, and it can also be easier to employ the technique without seeking any options for time-efficient methods for B_1^+ mapping. More importantly, as long as the two main assumptions are satisfied, we can retrospectively correct for B_1 effects in T_1 estimation in previously acquired data sets, which did not include B_1^+ mapping.

CONCLUSION

We have described a novel method that can efficiently measure both T_1 and B_1^+ maps when a constant-T1 reference region is available. The proposed method uses Dixon variable flip angle imaging, and B_1^+ maps are computed based on two major assumptions: the T_1 value of fat tissue is uniform and consistent across patients, and the fat region sufficiently covers the smoothly varying B_1^+ inhomogeneity across the region of interest. We have shown B_1^+ maps using the proposed method are similar to those using the conventional DAM and compensating for B_1^+ variation using RR-VFA can reduce T_1 estimation errors.

Acknowledgments

Grant Sponsors:

NIH R01-EB009055

References

1. Kuhl C. MRI of breast tumors. European radiology. 2000; 10:46–58. [PubMed: 10663717]
2. Hayes C, Padhani AR, Leach MO. Assessing changes in tumour vascular function using dynamic contrast-enhanced magnetic resonance imaging. NMR in Biomedicine. 2002; 15:154–163. [PubMed: 11870911]
3. Schabel MC, Parker DL. Uncertainty and bias in contrast concentration measurements using spoiled gradient echo pulse sequences. Phys Med Biol. 2008; 53:2345–2373. [PubMed: 18421121]
4. Tofts PS, Brix G, Buckley DL, Evelhoch JL, Henderson E, Knopp MV, Larsson HBW, Lee T-Y, Mayr NA, Parker GJM. Estimating Kinetic Parameters From Dynamic Contrast-Enhanced T1-Weighted MRI of a Diffusable Tracer: Standardized Quantities and Symbols. J Magn Reson Imaging. 1999; 10:223–232. [PubMed: 10508281]
5. Evelhoch JL. Key Factors in the Acquisition of Contrast Kinetic Data for Oncology. J Magn Reson Imaging. 1999; 10:254–259. [PubMed: 10508284]
6. Esserman L, Hylton N, Yassa L, Barclay J, Frankel S, Sickles E. Utility of magnetic resonance imaging in the management of breast cancer: evidence for improved preoperative staging. Journal of clinical oncology. 1999; 17:110–110. [PubMed: 10458224]
7. Hawighorst H, Weikel W, Knapstein PG, Knopp MV, Zuna I, Schönberg S, Vaupel P, van Kaick G. Angiogenic activity of cervical carcinoma: assessment by functional magnetic resonance imaging-based parameters and a histomorphological approach in correlation with disease outcome. Clinical cancer research. 1998; 4:2305–2312. [PubMed: 9796959]
8. Zahra MA, Hollingsworth KG, Sala E, Lomas DJ, Tan LT. Dynamic contrast-enhanced MRI as a predictor of tumour response to radiotherapy. The Lancet Oncology. 2007; 8:63–74. [PubMed: 17196512]
9. Deoni SCL, Rutt BK, Peters TM. Rapid combined T1 and T2 mapping using gradient recalled acquisition in the steady state. Magn Reson Med. 2003; 49:515–526. [PubMed: 12594755]

10. Brookes JA, Redpath TW, Gilbert FJ, Murray AD, Staff RT. Accuracy of T1 measurement in dynamic contrast-enhanced breast MRI using two-and three-dimensional variable flip angle fast low-angle shot. J Magn Reson Imaging. 1999; 9:163–171. [PubMed: 10077009]
11. Zhu X, Li K, Kamaly-Asl I, Checkley D, Tessier J, Waterton J, Jackson A. Quantification of endothelial permeability, leakage space, and blood volume in brain tumors using combined T1 and T2* contrast-enhanced dynamic MR imaging. J Magn Reson Imaging. 2000; 11:575–585. [PubMed: 10862055]
12. Wang HZ, Riederer SJ, Lee JN. Optimizing the precision in T1 relaxation estimation using limited flip angles. Magn Reson Med. 1987; 5:399–416. [PubMed: 3431401]
13. Treier R, Steingoetter A, Fried M, Schwizer W, Boesiger P. Optimized and combined T1 and B1 mapping technique for fast and accurate T1 quantification in contrast-enhanced abdominal MRI. Magn Reson Med. 2007; 57:568–576. [PubMed: 17326175]
14. Deoni SC. High-resolution T1 mapping of the brain at 3T with driven equilibrium single pulse observation of T1 with high-speed incorporation of RF field inhomogeneities (DESPOT1-HIFI). J Magn Reson Imaging. 2007; 26:1106–1111. [PubMed: 17896356]
15. Sung K, Daniel BL, Hargreaves BA. Transmit B1+ field inhomogeneity and T1 estimation errors in breast DCE-MRI at 3 Tesla. J Magn Reson Imaging. 201310.1002/jmri.23996
16. Greenman RL, Shirosky JE, Mulkern RV, Rofsky NM. Double Inversion Black-Blood Fast Spin-Echo Imaging of the Human Heart: A Comparison Between 1.5T and 3. 0T. J Magn Reson Imaging. 2003; 17:648–655. [PubMed: 12766893]
17. Sung K, Nayak KS. Measurement and characterization of RF nonuniformity over the heart at 3T using body coil transmission. J Magn Reson Imaging. 2008; 27:643–648. [PubMed: 18306272]
18. Kuhl CK, Kooijman H, Gieseke J, Schild HH. Effect of B1 inhomogeneity on breast MR imaging at 3. 0 T. Radiology. 2007; 244:929–930. [PubMed: 17709843]
19. Azlan CA, Di Giovanni P, Ahearn TS, Semple SIK, Gilbert FJ, Redpath TW. B1 transmission-field inhomogeneity and enhancement ratio errors in dynamic contrast-enhanced MRI (DCE-MRI) of the breast at 3T. J Magn Reson Imaging. 2010; 31:234–239. [PubMed: 20027594]
20. Di Giovanni P, Azlan C, Ahearn T, Semple S, Gilbert F, Redpath T. The accuracy of pharmacokinetic parameter measurement in DCE-MRI of the breast at 3 T. Physics in Medicine and Biology. 2010; 55:121. [PubMed: 20009182]
21. Insko, EK.; Bolinger, L. B1 mapping. Proc, SMRM, 11th Annual Meeting; Berlin. 1992. p. 4302
22. Cunningham CH, Pauly JM, Nayak KS. SDAM: Saturated double angle method for rapid B1+ mapping. Magn Reson Med. 2006; 55:1326–1333. [PubMed: 16683260]
23. Gupta, SN.; Schmidt, EJ.; Mulkern, R.; Fedorov, A.; Hancu, I.; Zhu, Y.; Tempany-Afdhal, C.; Fennessy, F. A Method for Correcting T1 maps of Prostate at 3T Obtained by Variable Flip Angle Imaging. Proc, ISMRM, 20th Annual Meeting; Melbourne. 2012. p. 1962
24. Rakow-Penner R, Daniel B, Yu H, Sawyer-Glover A, Glover GH. Relaxation times of breast tissue at 1. 5 T and 3T measured using IDEAL. J Magn Reson Imaging. 2006; 23:87–91. [PubMed: 16315211]
25. Ma J. Breath-hold water and fat imaging using a dual-echo two-point dixon technique with an efficient and robust phase-correction algorithm. Magn Reson Med. 2004; 52:415–419. [PubMed: 15282827]
26. Schär M, Vonken EJ, Stuber M. Simultaneous B0-and B1+-map acquisition for fast localized shim, frequency, and RF power determination in the heart at 3 T. Magn Reson Med. 2010; 63:419–426. [PubMed: 20099330]
27. Reeder SB, Pineda AR, Wen Z, Shimakawa A, Yu H, Brittain JH, Gold GE, Beaulieu CH, Pelc NJ. Iterative decomposition of water and fat with echo asymmetry and least-squares estimation (IDEAL): application with fast spin-echo imaging. Magn Reson Med. 2005; 54:636–644. [PubMed: 16092103]
28. de Bazelaire CM, Duhamel GD, Rofsky NM, Alsop DC. MR imaging relaxation times of abdominal and pelvic tissues measured in vivo at 3. 0 T: preliminary results. Radiology. 2004; 230:652–659. [PubMed: 14990831]
29. Sbrizzi A, Hoogduin H, Lagendijk JJ, Luijten P, van den Berg CA. Robust reconstruction of B1+ maps by projection into a spherical functions space. Magn Reson Med. 201310.1002/mrm.24640

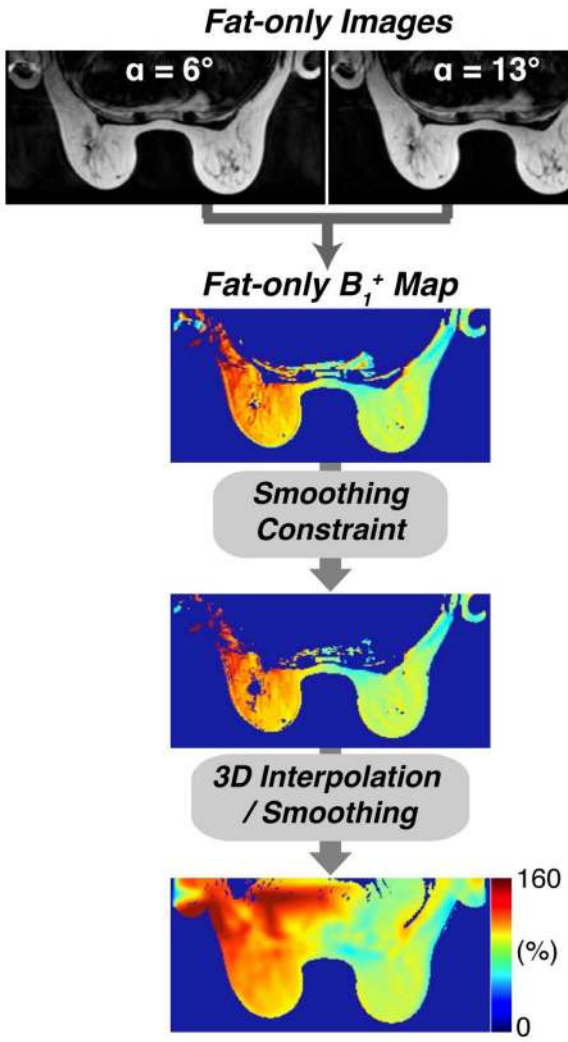

Figure 1.

A diagram of the proposed B_1^+ mapping using RR-VFA. After computing a fat-only B_1^+ map using the signal ratio of two fat-only images, the proposed method applies a smoothing constraint and 3D interpolation to construct the complete B_1^+ map.

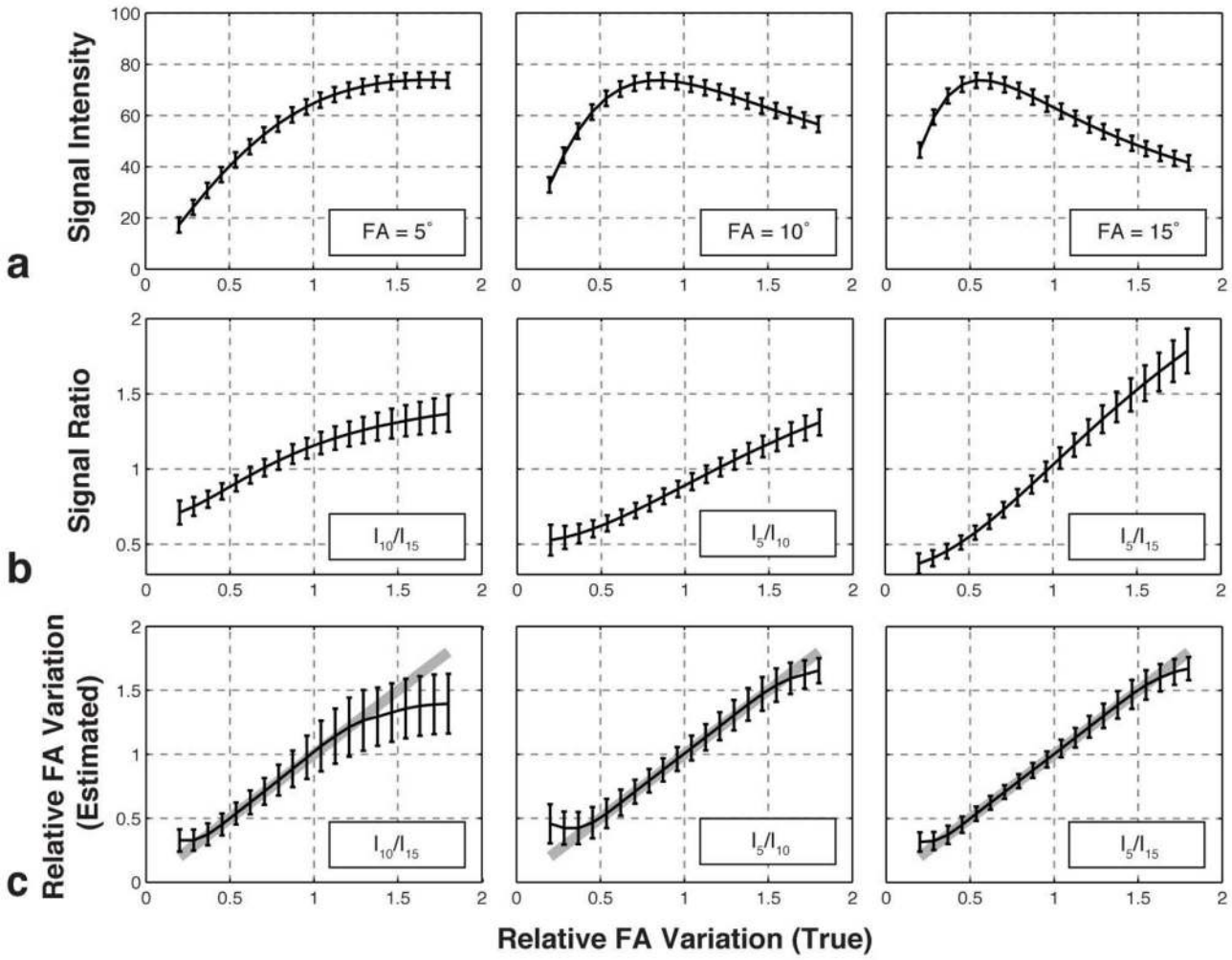

Figure 2.
Signal behavior of fat with (a) differing flip angles (5°, 10° and 15°) and (b) differing signal ratios (I_{10}/I_{15}, I_5/I_{10} and I_5/I_{15}), and (c) plots between the estimated and true flip angle variation for differing signal ratios (solid gray lines are the identity line). We added the same level of Gaussian noise to the simulated signal, and the plots are expressed as mean ± SD.

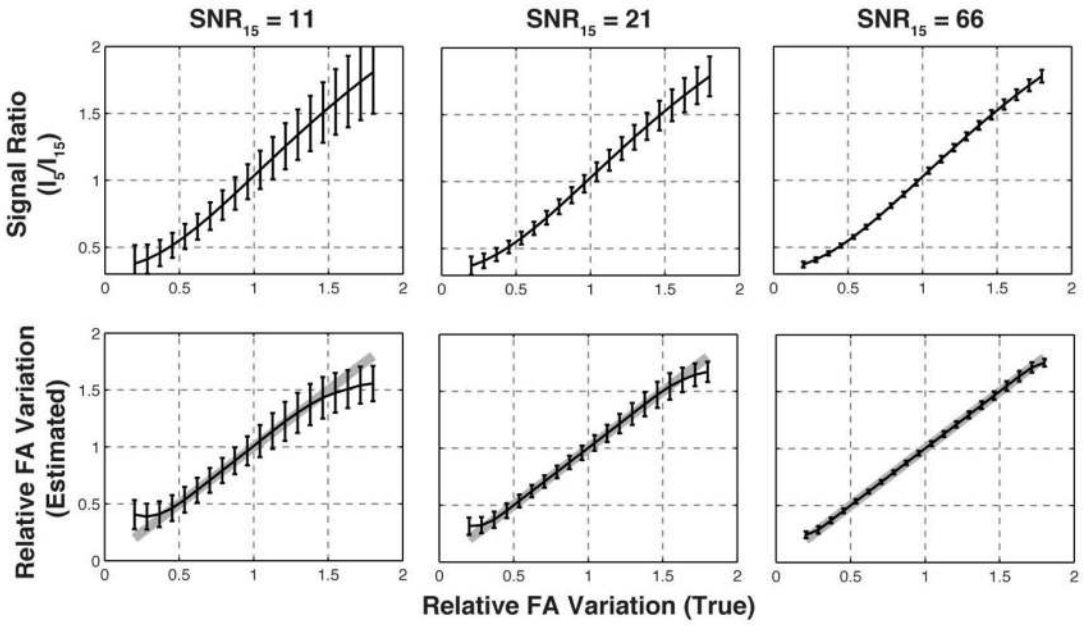

Figure 3.
Measurement accuracy of the RR-VFA B_1^+ mapping with different SNRs. SNR_{15} is the nominal SNR for 15°, and each plot for a different level of added Gaussian noise is expressed as mean ± SD.

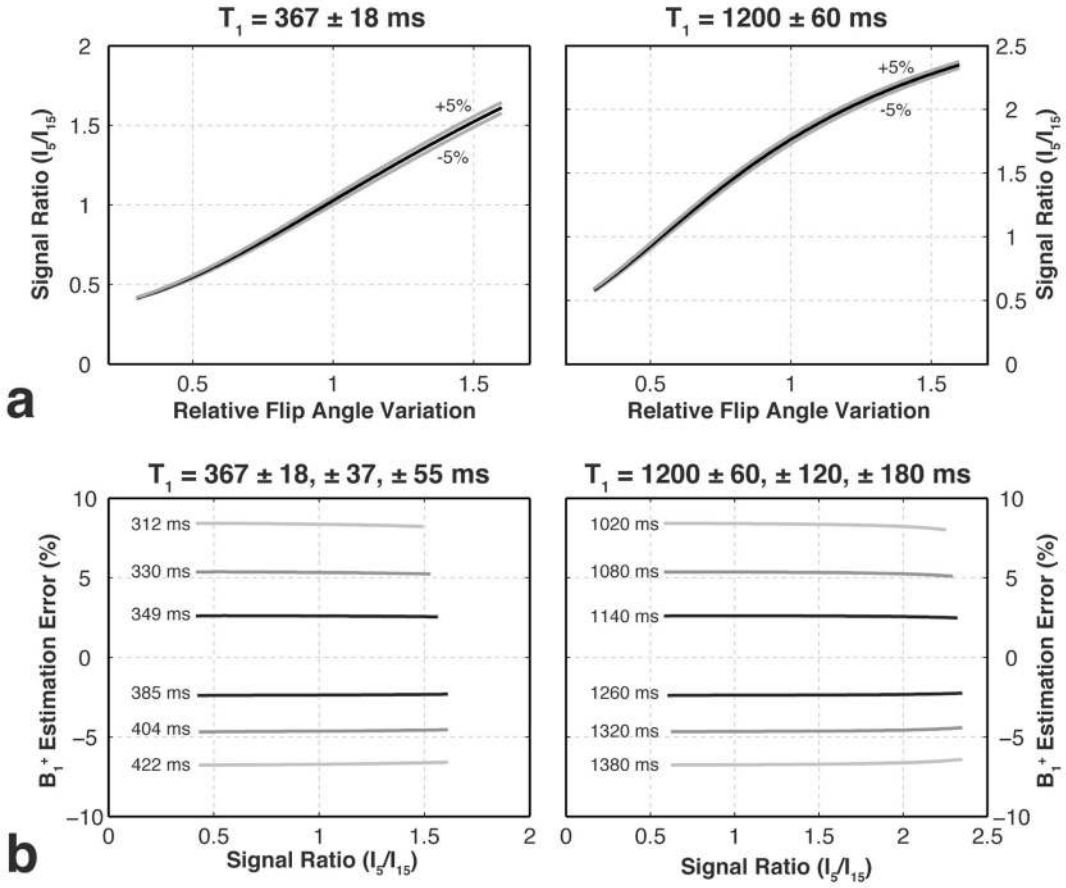

Figure 4.

B_1^+ estimation errors with different assumed T_1 values in the reference region for a true T_1 of 367 and 1200 ms. (a) The computed signal ratios with ± 5% variations of the true T_1 (gray lines), and (b) the overall B_1^+ estimation errors with different assumed T_1 values (± 5, 10 and 15% variations of the true T_1). When the assumed reference T_1 is longer than the true T_1 (positive variations of the true T_1), RR-VFA underestimates B_1^+ variation (negative errors).

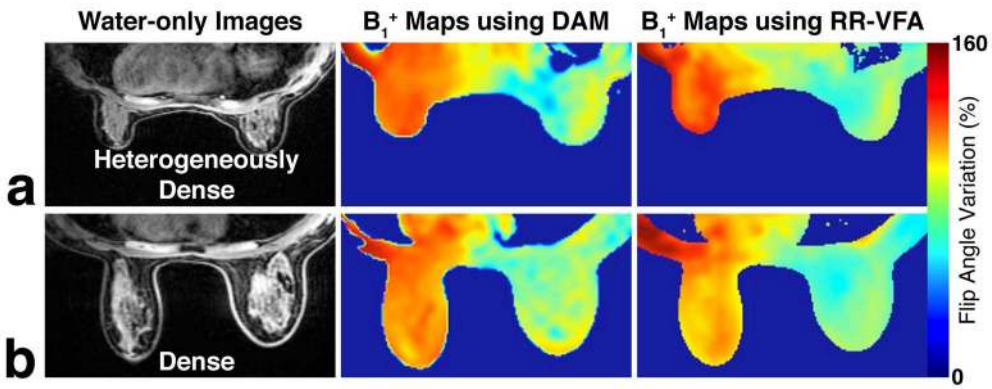

Figure 5.
Comparison of relative flip angle variation in percentage using DAM and RR-VFA on subjects with (a) heterogeneously dense and (b) dense breasts at 3T. The arrow shows a small region in the heart that does not have enough fatty tissue.

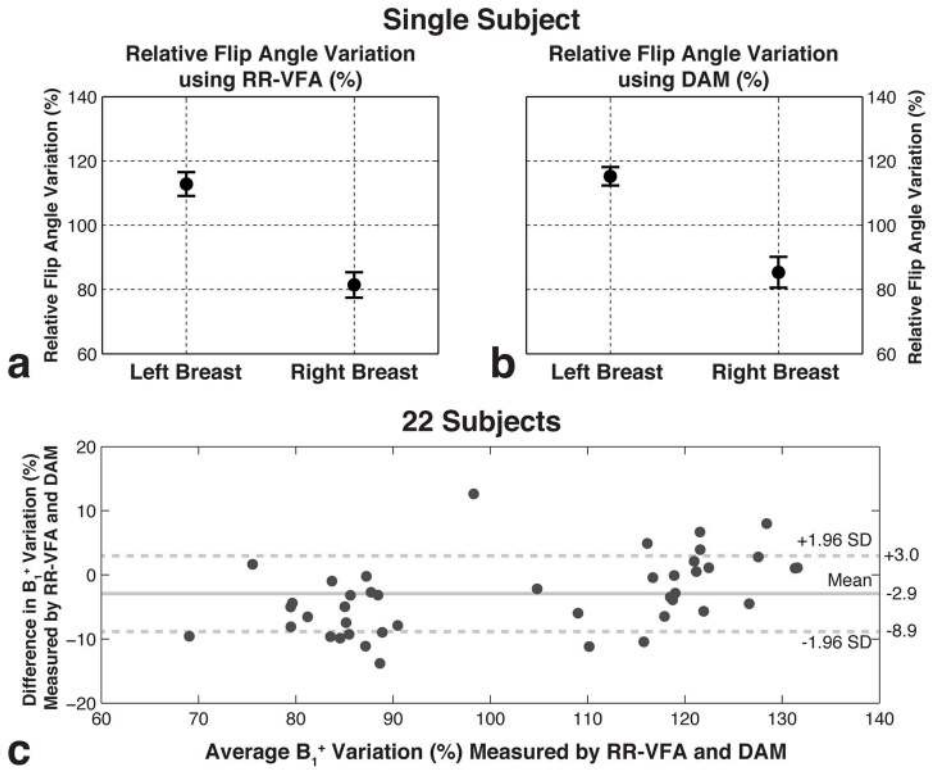

Figure 6.
Comparison of B_1^+ measurements using RR-VFA and DAM. (a and b) The mean and standard deviation plots for a single subject and (c) the Bland-Altman plot comparing B_1^+ maps in 22 subjects between RR-VFA and DAM methods.

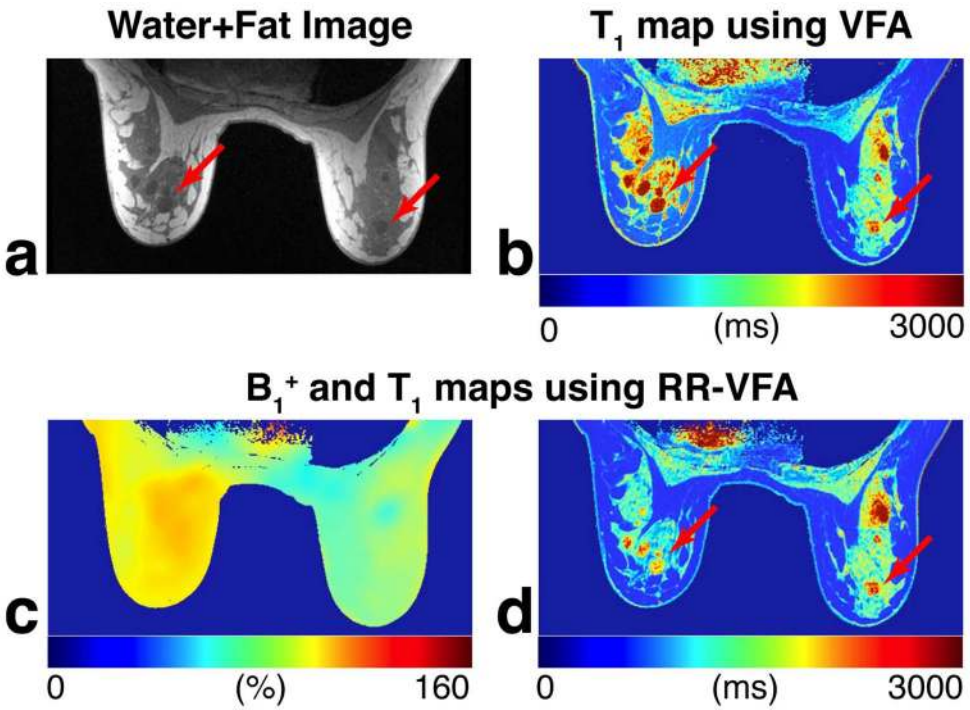

Figure 7.

High spatial resolution T_1 maps using VFA and RR-VFA. (a) The water+fat image for an anatomical reference, (b) the T_1 map using VFA (without compensating for B_1^+ inhomogeneity), and (c) the estimated B_1^+ map and the T_1 map with compensating for B_1^+ inhomogeneity using RR-VFA. The arrow shows heterogeneous T_1 of several breast masses.

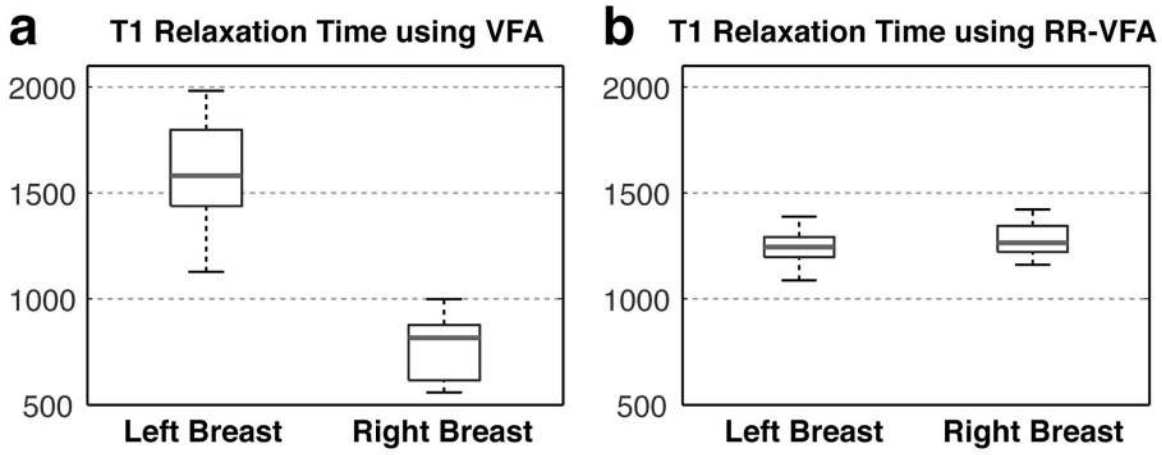

Figure 8.

Comparison of T_1 estimation in fibroglandular tissue using (a) standard VFA and (b) RR-VFA with correction of B_1^+ inhomogeneity in 6 breast MRI patients. The central mark on each box is the median, the edges of the box are the 25th and 75th percentiles, and the "whiskers" extend to the most extreme data points that were not considered outliers.